JOURNAL OF PROPULSION AND POWER
Vol. 9, No. 2, March–April 1993

Modal Simulation of Gear Box Vibration with Experimental Correlation

F. K. Choy* and Y. F. Ruan*
University of Akron, Akron, Ohio 44325
and
J. J. Zakrajsek† and F. B. Oswald†
NASA Lewis Research Center, Cleveland, Ohio 44135

A newly developed global dynamic model was used to simulate the dynamics of a gear noise rig at the NASA Lewis Research Center. Experimental results from the test rig were used to verify the analytical model. In this model, the number of degrees of freedom (DOF) of the system are reduced by transforming the system equations of motion into modal coordinates. The vibration of the individual gear-shaft systems is coupled through the gear-mesh forces. A three-dimensional bearing model was used to couple the casing structural vibration to the gear rotor dynamics. The system of modal equations is solved to predict the resulting vibration at several locations on the test rig. Experimental vibrational data were measured at several running speeds and were compared to the predictions of the global dynamic model. There was excellent agreement between the analytical and experimental vibration results.

Nomenclature

A = rotor modal displacement of X, θ_x
A_c = casing modal displacement of X_c, $X_{c\theta}$
B = rotor modal displacement of Y, θ_y
B_c = casing modal displacement of Y_c, $y_{c\theta}$
C_b = bearing damping matrix
$\bar{C}_b$ = $[\Phi]^T[C_b][\Phi]$
$\bar{\bar{C}}_b$ = $[\Phi_c]^T[C_b][\Phi_c]$
C_c = casing structure damping matrix
$\bar{C}_c$ = $[\Phi_c]^T[C_c][\Phi_c]$
D = rotor modal displacement of Z
D_c = casing modal displacement of Z_c, $Z_{c\theta}$
D_t = rotor modal displacement of θ_t
$F_c(t)$ = force acting on casing structure
$F_G(t)$ = gear force
$F_s(t)$ = shaft bow force = $[K_s]\{W_r\}$
$F(t)$ = external and mass-imbalance excitations
G_A = rotor angular acceleration
$\bar{G}_A$ = $[\Phi]^T[G_A][\Phi]$
G_v = gyroscopic
$\bar{G}_v$ = $[\Phi]^T[G_v][\Phi]$
I = identity matrix
K_A = $\frac{1}{2}\{[K_{bx}] + [K_{by}]\}$
$\bar{K}_A$ = $[\Phi]^T[K_A][\Phi]$
K_b = bearing stiffness
$\bar{K}_b$ = $[\Phi]^T[K_b][\Phi]$
$\bar{\bar{K}}_b$ = $[\Phi_c]^T[K_b][\Phi_c]$
K_c = casing structure stiffness
K_s = shaft bow stiffness
M = mass matrix of rotor
M_c = mass matrix of casing structure
W = generalized displacement vector of rotor
W_c = generalized displacement vector of casing
W_r = generalized displacement vector of the shaft bow
X, Y, Z = translational displacement in X, Y, Z direction
X_c, Y_c, Z_c = translational displacement of casing in X, Y, Z direction
$X_{c\theta}, Y_{c\theta}, Z_{c\theta}$ = translational displacement of casing in X, Y, Z direction
α = angle of orientation
$\theta_x, \theta_y, \theta_z$ = rotational displacement in X, Y, Z
μ = friction coefficient between the gear teeth surface
Φ = Eigenvector representing the mode shape
ω = critical speed of rotor
ω_c = critical speed of casing

Received May 5, 1992; presented as Paper 92-3494 at the AIAA 28th Joint Propulsion Conference, Nashville, TN, July 6–8, 1992; revision received Sept. 15, 1992; accepted for publication Oct. 6, 1992.

*Department of Mechanical Engineering.
†Research Engineer, Mechanical System Technology Branch.

I. Introduction

LARGE vibrations in gear transmission systems cause excessive wear and crack formation in gear teeth, which results in premature gear failure. With the need for higher operating speeds and power from transmission systems, the problem of excessive vibration becomes even more critical. In order to insure smooth and safe operation, it is necessary to understand the dynamics of the gear transmission system.

Two areas of research in the dynamics of gear transmission systems are 1) analytical simulation, and 2) experimental testing. There is a great deal of literature on the vibration analysis of a single gear stage.[1–6] Some work has been done on multistage gear vibration,[7–9] but very limited work[10,11] has been done on the dynamic analysis of gearbox vibration. Considerable effort has been devoted to experimentally studying gear dynamics[12–14] and localized vibration effects on gear teeth.[15] A few studies have been conducted to correlate analytically predicted and experimentally measured gearbox vibrations.

This article correlates the experimental results obtained from the test rig at the NASA Lewis Research Center with predictions from an analytical model developed by using the modal synthesis method.[7] The major excitations of the rotor system include mass imbalance, shaft residual bow, nonlinear gear-mesh forces[16] and gear-tooth frictional effects.[14] The vibratory motion between the rotor and the casing is coupled through the support bearing in the lateral and axial directions.[11] Gearbox mode shapes and vibration predictions from the analytical model are compared to those obtained from experimental testing.

II. Analytical Procedure

A. Development of Equations of Motion

The equations of motion each individual bear-shaft system can be written in matrix form[10,11] as

$$[M]\{\ddot{W}\} + [\dot{G}_v]\{\dot{W}\} + [G_A]\{W\} + [C_b]\{\dot{W} - \dot{W}_c\} + [K_b]\{W - W_c\} + [K_s]\{W - W_r\} = \{F(t)\} + \{F_G(t)\} \quad (1)$$

where the generalized displacement vector $\{W\}$ consists of the three displacement vectors, X, Y, Z, with the corresponding lateral θ_x, θ_y, and torsional θ_t rotational vectors as

$$\{W\} = \begin{Bmatrix} (X) \\ (\theta_x) \\ (Y) \\ (\theta_y) \\ (Z) \\ (\theta_t) \end{Bmatrix} \quad (2)$$

The equations of motion shown in Eq. (1) includes the effects of 1) inertia, $[M]$; 2) gyroscopic forces, $[G_v]$; 3) rotor angular acceleration, $[G_A]$; 4) bearing direct and cross-coupling damping, $[C_b]$; 5) bearing axial and lateral cross-coupling stiffness, $[K_b]$[12]; 6) casing vibration, $\{W - W_c\}$; 7) shaft residual bow, $\{W - W_r\}$; 8) external and mass-imbalance excitations, $\{F(t)\}$; and 9) nonlinear gear forces through gear mesh coupling, $\{F_G(t)\}$. For a multiple gear-shaft system, the equations of motion presented in Eq. (1) will be repeated for each individual shaft. The motions of the individual shafts are coupled to each other through the gear mesh forces and the shaft motions are coupled to the casing through the bearing stiffness $[K_b]$ and damping $[C_b]$.

The equations of motion for the casing can be written as where $\{W_c\}$ represents the generalized displacement vector of the casing structure

$$[M_c]\{\ddot{W}_c\} + [C_b]\{\dot{W}_c - \dot{W}\} + [K_b]\{W_c - W\} + [C_c]\{\dot{W}_c\} + [K_c]\{W_c\} = \{F_c(t)\} \quad (3)$$

$$\{W_c\} = \begin{Bmatrix} (X_c) \\ (X_{c\theta}) \\ (Y_c) \\ (Y_{c\theta}) \\ (Z_c) \\ (Z_{c\theta}) \end{Bmatrix} \quad (4)$$

The nonlinear gear forces for the Kth individual gear-shaft system, using nonlinear gear stiffness[6] and gear tooth friction,[15] are given as

x-Force

$$F_{Gxk} = \sum_{i=1, i\neq k}^{n} K_{tki}[-R_{ci}\theta_{ci} - R_{ck}\theta_{ck} + (X_{ci} - X_{ck})\cos\alpha_{ki} + (Y_{ci} - Y_{ck})\sin\alpha_{ki}] \cdot [\cos\alpha_{ki} + (\text{sign})(\mu)(\sin\alpha_{ki})] \quad (5)$$

y-Force

$$F_{Gyk} = \sum_{i=1, i\neq k}^{n} K_{tki}[-R_{ci}\theta_{ci} - R_{ck}\theta_{ck} + (X_{ci} - X_{ck})\cos\alpha_{ki} + (Y_{ci} - Y_{ck})\sin\alpha_{ki}] \cdot [\sin\alpha_{ki} + (\text{sign})(\mu)(\cos\alpha_{ki})] \quad (6)$$

Torsional

$$F_{Gtk} = \sum_{i=1, i\neq k}^{n} R_{ck}\{K_{tki}[(-R_{ci}\theta_{ci} - R_{ck}\theta_{ck}) + (X_{ci} - X_{ck})\cos\alpha_{ki} + (Y_{ci} - Y_{ck})\sin\alpha_{ki}]\} \quad (7)$$

where μ is the coefficient of friction between the gear tooth surface, "SIGN" is the unity sign function to provide the sign change when the mating teeth pass the pitch point,[15] subscript G represents force from gear, x, y, and t represent the direction, and k and i represent the rotor number for the driving and driven gear.

B. Modal Transformation

The equation of motion for the undamped rotor system is

$$[M]\{\ddot{W}\} + [[K_s] + [K_A]]\{W\} = 0 \quad (8)$$

with the average bearing support stiffness from the x-y direction[10,11] given as

$$[K_A] = \tfrac{1}{2}\{[K_{bx}] + [K_{by}]\} \quad (9)$$

The stiffness of the bearing support is assumed to be symmetrical in the development of the modal characteristics. The difference in stiffness are compensated by $[K_{bx} - K_A]$ value during solution of the global system in Eq. (18). The orthogonality condition for the orthonormal modes $[\Phi]$ are

$$[\Phi]^T[M][\Phi] = [I] \quad (10)$$

$$[\Phi]^T[K_s + K_A][\Phi] = [\omega^2] \quad (11)$$

Similarly, a set of orthogonality conditions can be derived for the casing equation of

$$[M_c]\{\ddot{W}_c\} + [C_c]\{\dot{W}_c\} + [K_c]\{W_c\} = 0 \quad (12)$$

with the orthonormal model $[\Phi_c]$ such that

$$[\Phi_c]^T[M_c][\Phi_c] = [I] \quad (13)$$

$$[\Phi_c]^T[C_c][\Phi_c] = [\tilde{C}_c] \quad (14)$$

$$[\Phi_c]^T[K_c][\Phi_c] = [\omega_c^2] \quad (15)$$

using modal transformation[10,11] by letting

$$\{W\} = \begin{Bmatrix} [\Phi_x]\{A\} \\ [\Phi_{x\theta}]\{A\} \\ [\Phi_y]\{B\} \\ [\Phi_{y\theta}]\{B\} \\ [\Phi_z]\{D\} \\ [\Phi_t]\{D_t\} \end{Bmatrix} \quad (16)$$

$$\{W_c\} = \begin{Bmatrix} [\Phi_{cx}]\{A_c\} \\ [\Phi_{cx\theta}]\{A_c\} \\ [\Phi_{cy}]\{B_c\} \\ [\Phi_{cy\theta}]\{B_c\} \\ [\Phi_{cz}]\{D_c\} \\ [\Phi_{cz\theta}]\{D_c\} \end{Bmatrix} \quad (17)$$

the equations of motion for the rotor (Eq. 1) can be transformed as

$$[I]\{\ddot{Z}\} + [\tilde{G}_v]\{\dot{Z}\} + [\tilde{G}_A]\{Z\} + [\tilde{C}_b]\{\dot{Z}\} - [\tilde{K}_b - \tilde{K}_A]\{Z\} + [\Phi]^T[C_b][\Phi_c]\{\dot{Z}_c\} + [\omega^2]\{Z\} - [\Phi]^T[K_B][\Phi_c]\{Z_c\} = [\Phi]^T\{F(t) + F_G(t) + F_s(t)\} \quad (18)$$

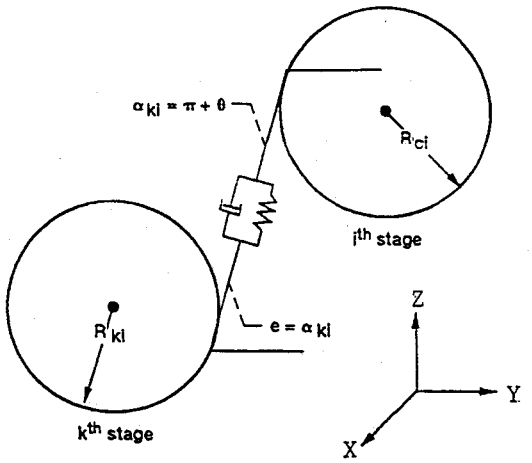

Fig. 1 Geometry of simulation of gear force.

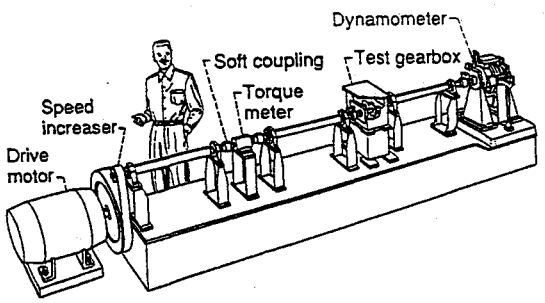

Fig. 2 Picture of the experimental gear noise rig.

and for the casing (Eq. 3) as

$$[I]\{\ddot{Z}_c\} + [\bar{C}_c]\{\dot{Z}_c\} + [\omega_c^2]\{Z_c\} + [\bar{\bar{K}}_b]\{Z_c\} + [\bar{\bar{C}}_b]\{\dot{Z}_c\} - [\Phi_c]^T[K_b][\Phi]\{Z\} - [\Phi_c]^T[C_b][\Phi]\{\dot{Z}\} = [\Phi_c]^T\{F_c(t)\} \tag{19}$$

where

$$\{Z\} = \begin{Bmatrix} \{A\} \\ \{B\} \\ \{D\} \\ \{D_t\} \end{Bmatrix} \{Z_c\} = \begin{Bmatrix} \{A_c\} \\ \{B_c\} \\ \{D_c\} \end{Bmatrix} \tag{20}$$

To develop the numerical transient analysis procedure, the initial boundary conditions for both rotor and casing (displacements and velocities) are used to evaluate the bearing and gear forces (Fig. 1) at the initial time. These forces and displacements are transformed into modal coordinates to solve the modal accelerations in Eqs. (18) and (19). A numerical integration scheme is used in integrating the modal accelerations to calculate the modal velocities and displacements for the next time step. The new modal velocities and displacements are used to calculate the system velocities and displacement in the generalized coordinates such that the bearing and gear forces can be evaluated at the new position. The nonlinear gear forces are evaluated through the relative motion between the two gear locations and the developed nonlinear gear mesh stiffness.[6] The process is repeated for the each time step in the transient analysis.

III. Experimental Study

The gear noise rig (Fig. 2) was used to measure the vibration, dynamic load, and noise of a geared transmission. The rig features a simple gearbox (Fig. 3) containing a pair of parallel axis gears supported by rolling element bearings. A 150-kW (200-hp) variable-speed electric motor powers the rig at one end, and an eddy-current dynamometer applies power-

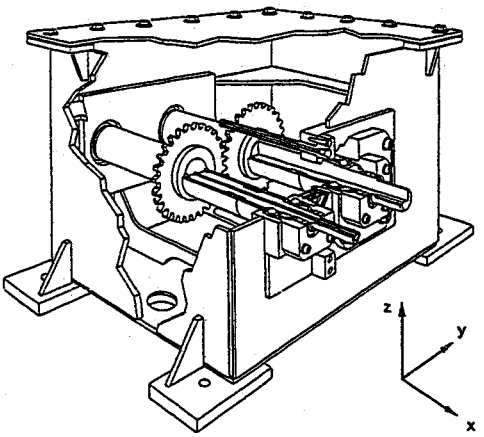

Fig. 3 Picture of the test gear box.

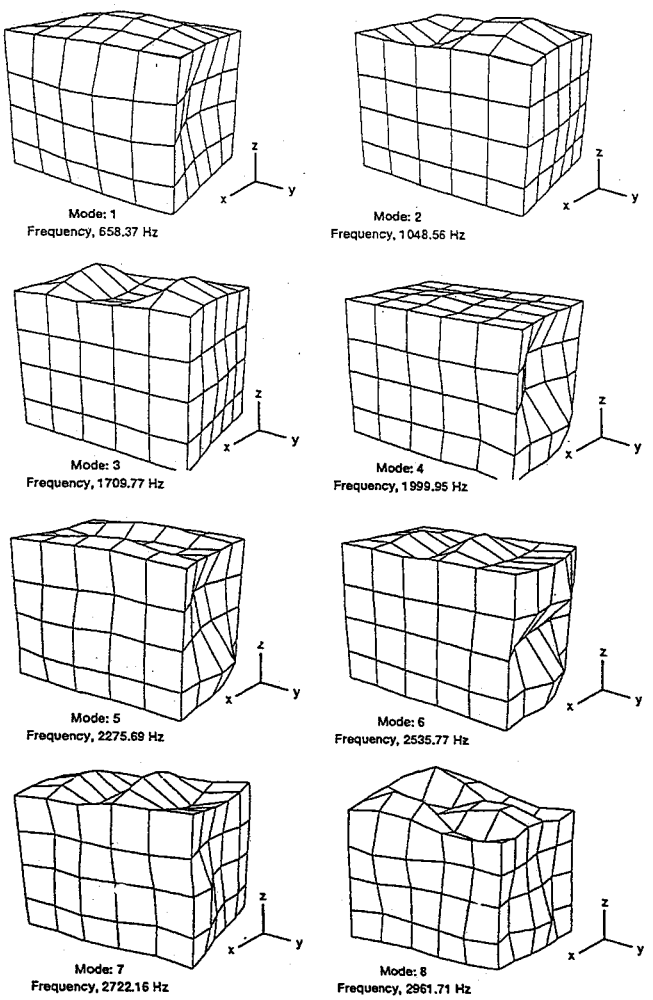

Fig. 4 Experimental gear box mode shapes.

Table 1 Test gear parameters

Gear type	Standard involute, full-depth tooth
Number of teeth	28
Module, mm (diametrial pitch in.$^{-1}$)	3.174(8)
Face width, mm (in.)	6.35(0.25)
Pressure angle, deg	20
Theoretical contact ratio	1.64
Driver modification amount, mm (in.)	0.023(0.0009)
Driven modification amount, mm (in.)	0.025(0.0010)
Driver modification start, deg	24
Driven modification start, deg	24
Tooth-root radius, mm (in.)	1.35(0.053)
Gear quality	AGMA class 13
Nominal (100%) torque, N-m (in.-lb)	71.77(635.25)

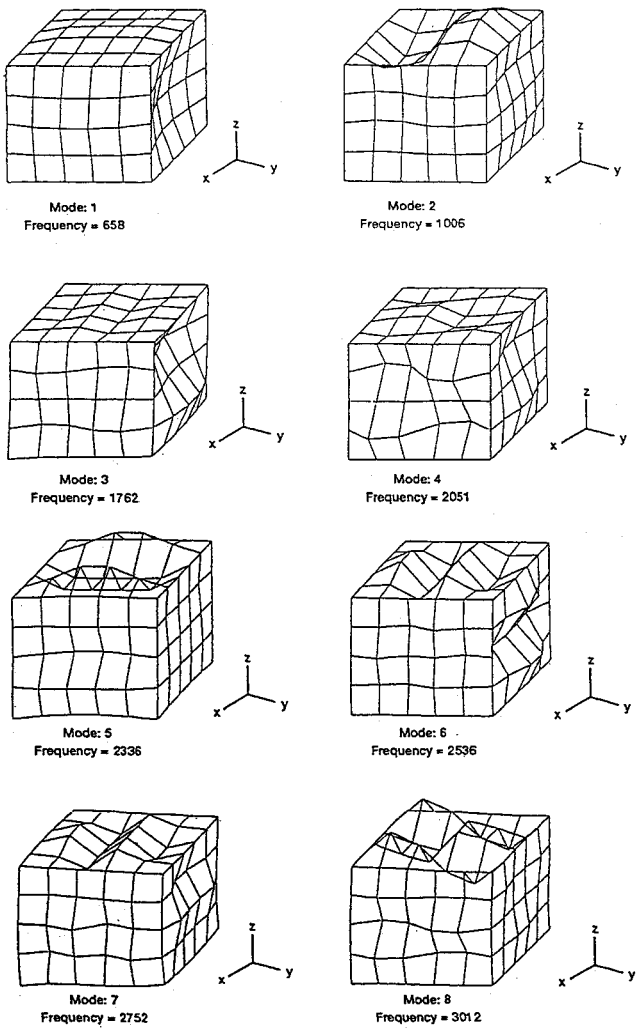

Fig. 5 X Direction experimental and analytical vibration frequency. Spectrum of the gearbox.

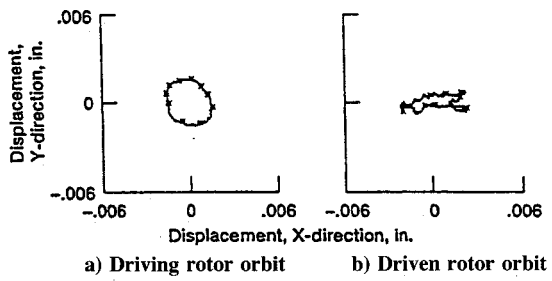

Fig. 6 Y Direction experimental and analytical vibration frequency. Spectrum of the gearbox.

absorbing torque at the other end. The test gear parameters are shown in Table 1.

Two sets of experiments were performed on the gearbox: 1) experimental modal analysis, and 2) dynamic vibration measurements during operation. In the experimental modal analysis, modal parameters, such as system natural frequencies and their corresponding mode shapes, were obtained through transfer function measurements using a two-channel dynamic signal analyzer and modal analysis software. For this experiment, 116 nodes were selected on the gearbox housing (Fig. 3). The measured three-dimensional mode shapes are presented in Fig. 4. The dynamic vibration measurements consist of data collected from accelerometers placed at three of the nodes on the surface of the casing. They were chosen such that vibration was measured in all three directions, x, y, and z. A dynamic signal analyzer was used to compute the

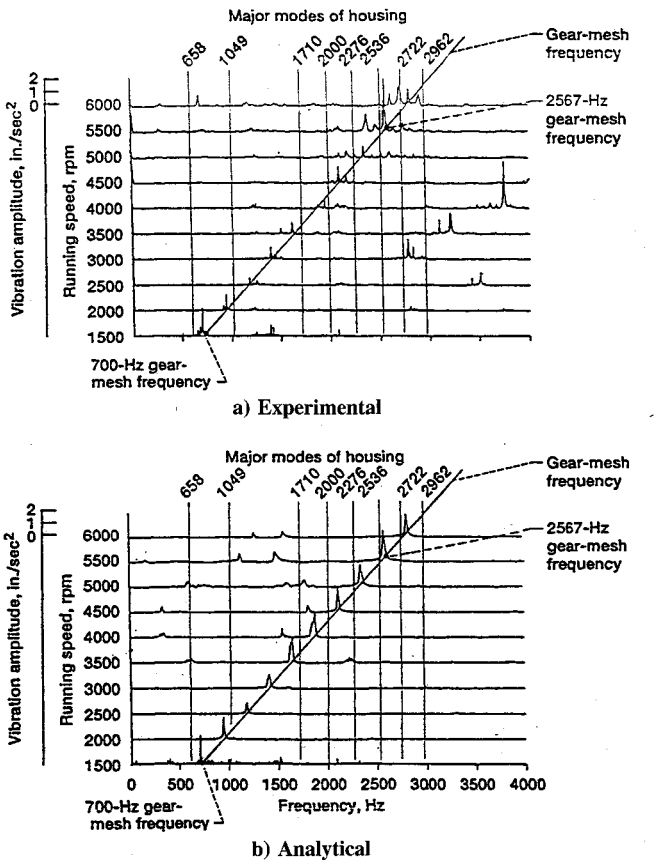

Fig. 7 Z Direction experimental and analytical vibration frequency. Spectrum of the gearbox.

frequency spectra of the vibration. The frequency spectra are given in Figs. 5a, 6a, and 7a, for the x, y, and z directions, respectively, for a number of different operating speeds.

IV. Discussion and Correlation of Results

The measured mode shapes, shown in Fig. 4, represent the major vibration modes of the gear noise rig in the 0–3-kHz region. Although these modes are only a small part of the total modes of the system, they represent the major part of the total global vibration of the system. In order to produce a compatible analytical simulation of the test apparatus, a similar set of modes were predicted by a finite-element model with beam and plate elements of the gearbox structure. This finite-element model serves as the basis for predicting casing vibrations in the overall global dynamic model. Out of a total of 25 modes found by the analytical model in the 0–3-kHz frequency region, the eight dominant modes were used to represent the gearbox dynamic characteristics. These simulated modes are shown in Fig. 8. The natural frequencies of the predicted modes are within 5% of the measured modes (Table 2), and the predicted mode shapes are very similar to the experimental modes shapes (Fig. 4). The correlation of results between the analytical model and the measurements confirms the accuracy of the dynamic representation of the test gearbox using only a limited number of modes.

For the dynamic study of the gearbox vibration, it was found that during a slow roll (low-speed run) of the rotor-gear assembly, a substantial residual bow, or eccentricity in the sleeve assembly, exists in the rotor system as shown by its large orbital motion given in Fig. 6. Figure 6a represents the orbit of the driver rotor at the gear location, and Fig. 6b represents that of the driven rotor. Note that the circular orbit in the driver rotor at low speed represents the residual bow deformation of the rotor. The elliptical orbit in the driven rotor is due to a combination of the residual bow effects and the vertical gear force from the torque of the driving rotor. In

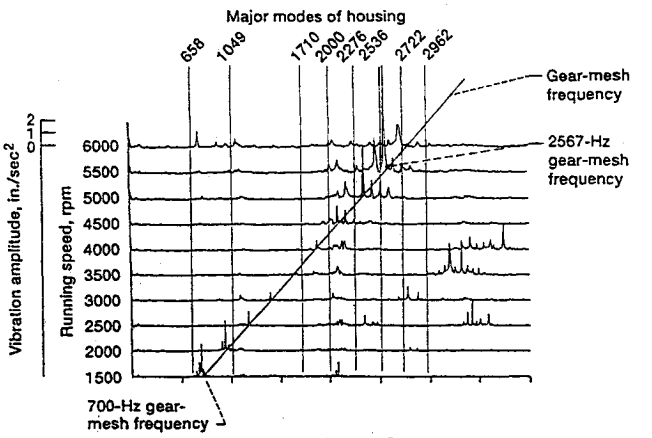

a) Experimental

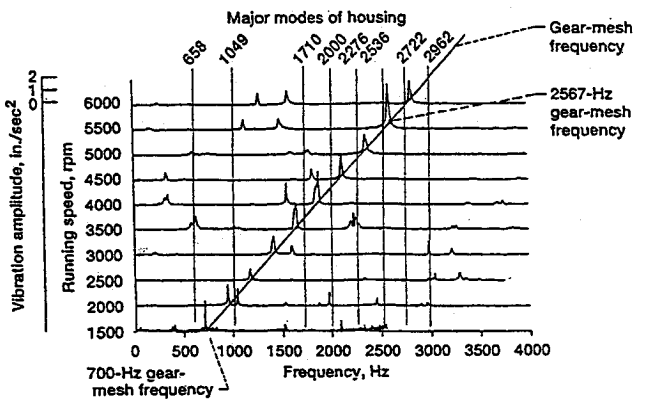

b) Analytical

Fig. 8 Analytical gear box mode shapes.

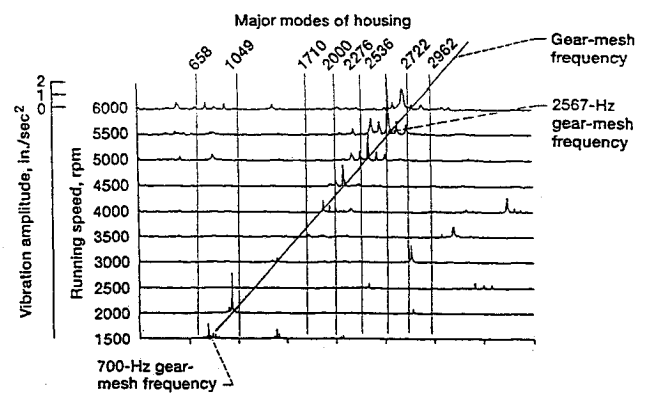

a) Experimental

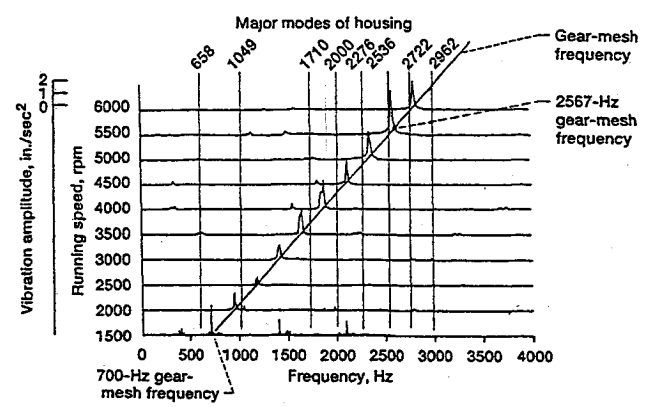

b) Analytical

Fig. 9 Orbital motion of rotor during slow roll.

Table 2 Comparison of experimentally measured and analytically modeled natural frequencies

Experimental, Hz	Analytical, Hz	Difference, %
658	658	0
1049	1006	−4.1
1710	1762	3.0
2000	2051	2.6
2276	2336	2.6
2536	1536	0
2722	2752	1.1
2962	3012	1.7

order to analytically simulate the influence of this effect, a residual bow of 2 mil (0.05 mm) is incorporated into the numerical model [Eq. (1)].

The frequency spectra of the analytically predicted casing vibration in the x, y, and z directions are presented in Figs. 7b, 8b, and 9b, respectively. As seen in Fig. 7a, the experimental casing vibration in the x direction shows a major vibration component at the gear mesh frequency (28 × shaft speed), at each rotational speed. A closer examination of this component shows that two major vibration peaks occur at the running speeds of 1500 rpm (at a tooth-pass frequency of 700 Hz) and 5500 rpm (at a tooth-pass frequency of 2560 Hz). These peaks are a result of the tooth-pass frequency exciting two of the major natural frequencies of the housing, namely the 658 and 2536 Hz modes. However, the presence of other modes can be seen (the 658 and 2536 Hz modes), and dominate the spectra when excited by the gear mesh frequency.

When comparing the predicted vibration spectra with the measured spectra, it was found that although the actual amplitude values did not always agree, the general trends of the spectra were very similar. The predicted vibration spectra of the housing in the x direction is given in Fig. 7b. In comparing Figs. 7a and 7b, the predicted amplitude at the gear mesh frequency at 1500 rpm is only 3% above the measured value. The comparison at 5500 rpm is not that close, where the predicted amplitude is 38% below the measured value. In comparing trends, the predicted spectra show the same gear mesh frequency induced excitation of the 658 and 2536 Hz modes as found in the measured spectra, at the running speeds of 1500 and 5500 rpm, respectively.

Figures 8a and 8b, and Figs. 9a and 9b present the comparison of predicted and measured housing vibration spectra in the y and z directions, respectively. The results of the comparison are the same as those presented for the housing vibration in the x direction (Figs. 7a and 7b). Actual values of the components in the spectra were not always in good agreement, however, the general trends between the predicted and measured housing vibration spectra were very similar. Also, as seen in Fig. 9b, at the 1500 rpm speed, the model predicts the second and third harmonic of the gear mesh frequency. As shown in Fig. 8a, the measured vibration confirms the presence of these two harmonics at the 1500 rpm running speed.

V. Conclusions

A newly developed global dynamic model was used to simulate the dynamics of a simple transmission system. Predicted casing vibrations were compared to measured results from a typical gear noise test rig. The conclusions of this study are summarized as follows:

1) The dynamics of the housing can be accurately modeled with a limited amount of analytically predicted, experimentally verified vibration modes of the structure.

2) The global dynamic model is capable of including in the analysis the effects of shaft residual bow.

3) The characteristics and trends of the housing vibration spectra predicted by the global dynamic model are the same or very similar to those found in the experimental data.

References

[1]August, R., and Kasuba, R., "Torsional Vibrations and Dynamic Loads in a Basic Planetary Gear System," *Journal of Vibration, Acoustic, Stress, and Reliability in Design*, Vol. 108, No. 3, 1986, pp. 348–353.

[2]Choy, F. K., Townsend, D. P., and Oswald, F. B., "Dynamic Analysis of Multimesh-Gear Helicopter Transmissions," NASA TP2789, Feb. 1988.

[3]Cornell, R. W., "Compliance and Stress Sensitivity of Spur Gear Teeth," *Journal of Mechanical Design*, Vol. 103, No. 2, 1981, pp. 447–459.

[4]Lin, H., Houston, R. L., and Coy, J. J., "On Dynamic Loads in Parallel Shaft Transmissions," NASA TM100108, Dec. 1987.

[5]Mark, W. D., "The Transfer Function Method for Gear System Dynamics Applied to Conventional and Minimum Excitation Gear Design," NASA CR-3626, Oct. 1982.

[6]Boyd, L. S., and Pike, J. A., "Epicyclic Gear Dynamics," *AIAA Journal*, Vol. 27, No. 5, 1989, pp. 603–609.

[7]Choy, F. K., Townsend, D. P., and Oswald, F. B., "Experimental and Analytical Evaluation of Dynamic Load and Vibration of a 2240-KW Rotor Craft Transmission," *Journal of The Franklin Institute*, Vol. 326, No. 5, 1989, pp. 721–735.

[8]David, J. W., Mitchell, L. D., and Daws, J. W., "Using Transfer Matrices for Parametric System Forced Response," *Journal of Vibration, Acoustics, Stress and Reliability in Design*, Vol. 109, No. 4, 1987, pp. 356–360.

[9]Ozguven, H. N., and Houser, D. R., "Mathematical Models Used in Gear Dynamics—A Review," *Journal of Sound and Vibration*, Vol. 121, No. 3, 1988, pp. 383–411.

[10]Choy, F. K., Tu, Y. K., Savage, M., and Townsend, D. P., "Vibration Signature Analysis of Multistage Gear Transmission," *Journal of the Franklin Institute*, Vol. 328, Nos. 2 and 3, 1991, pp. 281–299.

[11]Choy, F. K., Ruan, Y. F., Zakrajsek, J. J., Oswald, F. B., and Coy, J. J., "Analytical and Experimental Study of Vibrations in a Gear Transmission," AIAA 27th Joint Propulsion Conf., AIAA Paper 91-2019, Sacramento, CA, June 24–27, 1991.

[12]Lim, T. C., Signh, R., and Zakrajsek, J. J., "Modal Analysis of Gear Housing and Mounts," *7th International Modal Analysis Conference*, Vol. 2, Society of Experimental Mechanics, Bethel, CT, 1990, pp. 1072–1078.

[13]Lewicki, D. G., and Coy, J. J., "Vibration Characteristics of the OH-58A Helicopter Main Rotor Transmission," NASA TP-2705, April 1987.

[14]Oswald, F. B., "Gear Tooth Stress Measurements on the UH-60A Helicopter Transmission," NASA TP-2698, March 1987.

[15]Rebbechi, B., Oswald, F. O., and Townsend, D. P., "Dynamic Measurements of Gear Tooth Friction and Load," NASA TM-103281, Oct. 1991.

[16]Townsend, D. P., and Bamberger, E. N., "Surface Fatigue Life of M50NiL and AISI9310 Spur Gears and R C Bars," *Proceedings of the 1991 International Conference on Motion and Power Transmissions*, Hiroshima, Japan, Nov. 24–26, 1991, pp. 855–860.